

The early phases of galaxy clusters formation in IR: coupling hydrodynamical simulations with GRASIL3D

Gian Luigi Granato^{1*}, Cinthia Ragone-Figueroa^{2,1†}, Rosa Domínguez-Tenreiro³, Aura Obreja³, Stefano Borgani^{1,4}, Gabriella De Lucia¹ and Giuseppe Murante¹

¹ *Istituto Nazionale di Astrofisica INAF, Osservatorio Astronomico di Trieste, Via Tiepolo 11, I-34131 Trieste, Italy*

² *Instituto de Astronomía Teórica y Experimental (IATE),*

Consejo Nacional de Investigaciones Científicas y Técnicas de la República Argentina (CONICET),

Observatorio Astronómico, Universidad Nacional de Córdoba, Laprida 854, X5000BGR, Córdoba, Argentina

³ *Depto. de Física Teórica, Universidad Autónoma de Madrid, E-28049 Cantoblanco Madrid, Spain*

⁴ *Astronomy Unit, Department of Physics, University of Trieste, via Tiepolo 11, I-34131 Trieste, Italy*

Accepted ASAP; Received in original form ASAP

ABSTRACT

We compute and study the infrared and sub-mm properties of high redshift ($z \gtrsim 1$) simulated clusters and proto-clusters, by coupling the results of a large set of hydro-dynamical zoom-in simulations including active galactic nuclei (AGN) feedback (Ragone-Figueroa et al. 2013), with the recently developed radiative transfer code GRASIL3D (Dominguez-Tenreiro et al. 2014), which accounts for the effect of dust reprocessing in an arbitrary geometry, and we customized for the present purpose.

While this field is in its infancy from the observational point of view, a rapid development is expected in the near future, thanks to observations performed in the far IR and sub-mm bands. Notably, we find that in this spectral regime our prediction are little affected by the assumption required by this post-processing, and the emission is mostly powered by star formation rather than accretion onto super massive black hole (SMBH).

The comparison with the little observational information available so far, highlights that the simulated cluster regions never attain the impressive star formation rates suggested by these observations. This problem becomes more intriguing taking into account that the brightest cluster galaxies (BCGs) in the same simulations turns out to be too massive (Ragone-Figueroa et al. 2013). It seems that the interplay between the feedback schemes and the star formation model should be revised, possibly incorporating a positive feedback mode.

Key words: galaxies: clusters: general - hydrodynamics - radiative transfer - dust, extinction - submillimetre: galaxies - infrared: galaxies

1 INTRODUCTION

Galaxy clusters are fundamental probes for many questions of extra-galactic astrophysics and cosmology, both from the observational as well as from the theoretical point of view (for a recent review see Kravtsov & Borgani 2012). Their properties are relatively well known at low redshift $z \lesssim 1$. In particular, it is well assessed that the central regions of massive clusters are characterized by a population of passive early type galaxies, whose stellar population is old,

having formed at $z \gtrsim 2$. More debated and uncertain is the main epoch in which these stars assembled into the single galactic units we see in the local universe. Indeed, there seems to be some disagreement between the relatively important role of merging below $z \lesssim 1$ expected on the basis of recent theoretical computations (Guo et al. 2011; Johansson, Naab, & Ostriker 2012), and some observational constraints (Stott et al. 2011; Lidman et al. 2012; Lin et al. 2013; Inagaki et al. 2014). Unsurprisingly, a proper theoretical understanding of this and other questions concerning the evolution of galaxy population in clusters, requires a treatment of the various processes driving it, such as star formation, AGN activity, feedback, dynamical interactions,

* Email: granato@oats.inaf.it

† Email: cin@oac.unc.edu.ar

at a much deeper level than presently feasible. Galaxy clusters over cosmic time are prime laboratories for these processes acting together, which results in a clear environment dependence of the basic properties of galaxies, and of their evolutionary history.

At $z \gtrsim 1$, a regime approaching the formation epoch of massive clusters, observational studies become more and more problematic and, as a consequence, scarce. The identification of clusters (or proto-clusters, somewhat loosely defined as systems that exhibit a significant over-density of galaxies, not yet gravitationally bound, but that may collapse to form a cluster at later time) becomes difficult, due both to increasing detection challenges and intrinsic rareness. Also, a detailed determination of the properties of their galaxies is progressively uncertain.

Nevertheless, the study of high z clusters is now an active field of research, as testified by the fact that even the redshift barrier of $z=1.5$ has been broken in the last few years, by means of mid infrared or X-ray selection, albeit by just a handful of examples so far. These observations suggest that, while galaxy populations in the centers of massive clusters show little change out to $z \simeq 1.4$ (Mei et al. 2009; Strazzullo et al. 2010), in high redshifts clusters $z \gtrsim 1.5$, intense star formation becomes common, even in the cores and in most massive galaxies (Tran et al. 2010; Hilton et al. 2010; Hayashi et al. 2011; Santos et al. 2011; Fassbender et al. 2014; Dannerbauer et al. 2014; Santos et al. 2014a,b). For instance, Tran et al. (2010), considering only the IR luminous galaxies in the core (projected distances $< 0.5\text{Mpc}$) of a *Spitzer*-selected cluster at $z = 1.62$, found that the star formation rate density to be at least $1700 \text{ M}_{\odot} \text{ yr}^{-1} \text{ Mpc}^{-2}$. This estimate has been later revised downward by Santos et al. (2014a) to $990 \pm 120 \text{ M}_{\odot} \text{ yr}^{-1} \text{ Mpc}^{-2}$, with a contribution from the BCG of $256 \pm 70 \text{ M}_{\odot} \text{ yr}^{-1}$. Santos et al. (2014b) measured a strikingly high amount of star formation $\sim 2000 \text{ M}_{\odot} \text{ yr}^{-1}$ in the inner 250 kpc of a massive ($\sim 5 \times 10^{14} \text{ M}_{\odot}$) cluster at $z \sim 1.6$. Dannerbauer et al. (2014), using APEX LABOCA $870 \mu\text{m}$ observations of the field around the so-called spiderweb radio galaxy at $z=2.16$, widely studied as a signpost for a massive cluster in formation, measured a SFR density of $\sim 1500 \text{ M}_{\odot} \text{ yr}^{-1} \text{ Mpc}^{-3}$, occurring within a region of 2 Mpc. On the other hand, there are also examples of high redshift clusters ($z \gtrsim 2$) with a mixed population comprising both quiescent, structurally evolved galaxies, as well as star forming ones (Strazzullo et al. 2013; Gobat et al. 2013), or even clusters dominated by quiescent early type galaxies (Tanaka et al. 2013). In any case, it has been reported a reversal of the SFR-density relation, showing increasing SFR with increasing local density at $z \gtrsim 1$, both in the field as well as in higher density environments (Elbaz et al. 2007; Cooper et al. 2008; Tran et al. 2010; Santos et al. 2014a,b).

To shed light directly on the history of assembly of galaxy clusters, it is clear that larger samples are highly demanded at high redshift, greater than $1 - 1.5$, selected with techniques enabling the discovery of clusters or proto-clusters in various evolutionary stages. A widely used method to discover high redshift clusters has been to look for the effects of their hot gas component, namely its X-ray emission or the SZ effect it produces on the cosmic microwave background. The former type of selection becomes

rapidly inefficient at $z \gtrsim 1.5$, due to sensitivity limitations, and both requires massive and well relaxed structures, whose number density is expected to be rapidly declining at such early cosmic epochs. A complementary possibility, which has been exploited in the past few years, is to preselect overdensities of galaxies whose near infrared photometric properties are characteristic of high redshift systems. These overdensities require later spectroscopic confirmation. At $z > 2$ most efforts have been devoted in the search of protoclusters using as tracers high- z giant radiogalaxies (e.g. Hatch et al. 2011; Rigby et al. 2014; Dannerbauer et al. 2014).

A recently explored alternative to select high z clusters of galaxies has been used by Clements et al. (2014), taking advantage of the well assessed efficiency of far-IR/sub-mm surveys in detecting high- z objects in a violent, dust obscured, star forming phase (e.g. Coppin et al. 2006, and references therein). These authors, following the suggestion by Negrello et al. (2005), tested the idea of exploiting the all sky coverage of the Planck satellite survey, in order to detect candidate clusters undergoing a pristine and violent star forming phase. These are expected to show up as cold compact sources, significantly contributing to the Planck number counts, which can be later confirmed as clumps of high- z galaxies by means of higher angular resolution maps produced by the Herschel satellite. In this first demonstrative study, Clements et al. (2014) uncovered four such sources looking just at the $\sim 90 \text{ sq. deg.}$ of sky observed by Herschel as part of the HerMES survey.

The main purpose of this paper is to compare these findings with the predictions of our high resolution simulations of the formation of massive galaxy clusters (e.g. Ragone-Figueroa et al. 2013; Planelles et al. 2014). To do this, we post-process the simulation results at high $z \gtrsim 1$ with GRASIL-3D (Domínguez-Tenreiro et al. 2014), a recently developed fully three dimensional radiative transfer code, which computes the dust reprocessing of the primary photons emitted by stellar populations (or other sources), and it has been developed specifically to deal with the output of simulations. This post-processing is of course required in order to properly compare with observations at IR or sub-mm wavelengths. We discuss to what extent the spectrophotometric properties of the cluster region are robust against reasonable variations of GRASIL-3D assumptions, in the various spectral regions. We incorporate in GRASIL-3D a consistent treatment of the radiative effect of AGN activity (our simulations include AGN feedback), which allows us to predict its contribution to the emitted specific luminosity.

Besides GRASIL-3D a few other tools exist with similar capabilities, and have been coupled with simulations output, e.g.: the later version of SUNRISE (Jonsson, Groves, & Cox 2010); RADISHE (Chakrabarti & Whitney 2009); ART2 (Li et al. 2008) and SKIRT (Camps & Baes 2014). All but GRASIL-3D, which uses ray-tracing and finite difference, use Monte Carlo techniques to follow the transfer of photons through the diffuse ISM, and hence the dust re-emission. However, to the best of our knowledge, this is the first time that this post-processing has been applied to galaxy clusters as a whole.

The paper is organized as follows: Section 2 is devoted to a brief description of the simulations set, and contains ref-

ferences to previous papers, wherein all the details can be retrieved; in Section 3 the radiative code used to post-process the simulations, GRASIL-3D, is described, including a few modifications introduced specifically for the purposes of this paper; the results are presented and discussed in Section 4, and summarized in the final Section 5.

2 THE SIMULATIONS

For this work we used simulations of 24 Lagrangian regions extracted from a low resolution N-body simulation within a cosmological box of $1h^{-1}\text{Gpc}$ comoving size. We assumed a flat Λ CDM cosmology with the following parameters: matter density parameter $\Omega_m = 0.24$; baryon density parameter $\Omega_b = 0.04$; Hubble constant $h = 0.72$; normalization of the power spectrum $\sigma_8 = 0.8$; primordial power spectral index $n_s = 0.96$. The Lagrangian regions surround the most massive halos identified at $z = 0$ in the parent simulation, all having virial mass¹ of at least $10^{15}h^{-1}M_\odot$ (e.g. Bonafede et al. 2011). Initial conditions for the hydrodynamical simulations have been created by increasing mass resolution within such regions, and adding the corresponding high-frequency Fourier modes from the linea power spectrum of the adopted cosmological model. In The mass of DM particles is $8.47 \times 10^8 h^{-1}M_\odot$, and the initial mass of each gas particle is $1.53 \times 10^8 h^{-1}M_\odot$.

Our simulations were performed using the TreePM-SPH GADGET-3 code, an improved version of GADGET-2 (Springel 2005). The force accuracy, in the high resolution regions, is set by $\epsilon = 5h^{-1}\text{ kpc}$ for the Plummer-equivalent softening parameter, fixed in comoving units at redshifts > 2 and fixed in physical units in the redshift range $2 \leq z \leq 0$. When computing hydrodynamical forces, the minimum value attainable for the Smoothed Particle Hydrodynamics (SPH) smoothing length of the B-spline kernel is set to half of the gravitational softening length.

The simulations used in this work include gas cooling, star formation, supernova feedback and AGN feedback. For a detailed description of the sub-resolution models we refer the reader to Ragone-Figueroa et al. (2013) and Planelles et al. (2014). In particular, the former paper contains a discussion of the prescriptions for the BH feedback, which is based on the simple recipe put forward by Springel et al. (2005) and adopted in many simulations, but for a few important modifications. These were required because the latter model was thought and calibrated for non-cosmological high resolution simulations of merging galaxies, and it leads, in the context of our simulations, to several unwanted and misleading effects, such as unrealistic merging of distant SMBH particles or losses of the energy produced by accretion.

Since some concepts of this modelling are used in Section 3, to facilitate the reading we recall that the BHs are represented by means of collision-less particles, subject only to gravitational forces, and growing by accretion and

merging. The accretion rate is given by the minimum between a Bondi accretion rate, modified by the inclusion of a multiplicative factor, and the Eddington limit. The former is loosely thought as providing an estimate of how the gas available for accretion scales with the conditions in the BHs surroundings, while the Eddington limit ensures that the produced radiation pressure does not overcome gravity. When two BH particles are within the gravitational softening and their relative velocity is smaller than a fraction 0.5 of the sound velocity of the surrounding gas, we merge them. The accretion onto SMBHs produces an energy determined by a parameter $\epsilon_r = 0.2$, giving the fraction of accreted mass converted to energy. Another parameter $\epsilon_f = 0.2$ defines the fraction of this energy that is thermally coupled to the surrounding gas. As usual, we calibrated these parameters in order to reproduce the observed scaling relations of SMBH mass in spheroids at $z=0$.

For the analysis presented in this paper, we identified cluster progenitors at several redshifts $z \leq 3$. In particular, Our sample has a median virial mass of $8 \times 10^{13} h^{-1} M_\odot$ and $2 \times 10^{14} h^{-1} M_\odot$ at $z = 2$ and 1, respectively. The corresponding median SFRs within the virial radii are of 800 and 500 $M_\odot \text{ yr}^{-1}$.

2.1 Cluster selection and initial conditions

As described in full details in Bonafede et al. (2011), the 24 most massive clusters, in terms of FOF mass, have been identified and selected in the parent simulations at $z=0$. The re-simulations at higher resolution have been carried out using the *Zoomed Initial Conditions* technique (Tormen, Bouchet, & White 1997). The HR regions allow to identify other 50 less massive and interesting clusters, uncontaminated by low resolution particles, which have been studied in several papers (e.g. Ragone-Figueroa et al. 2013; Planelles et al. 2014). However, here we focus only on the 24 originally selected one, because they constitute a statistically well defined sample, whose final virial mass is in the ranges between $\simeq 1$ and $3 \times 10^{15} h^{-1} M_\odot$ (see table 1 in Bonafede et al. 2011). Our sample has a median virial mass of $8 \times 10^{13} h^{-1} M_\odot$ and $2 \times 10^{14} h^{-1} M_\odot$ at redshift 2 and 1 respectively, and the corresponding median SFRs within the virial radius are of 800 and 500 $M_\odot \text{ yr}^{-1}$.

3 GRASIL-3D AND ITS MODIFICATIONS

In order to perform radiative transfer calculations in the region of simulated clusters, we use GRASIL-3D (Domínguez-Tenreiro et al. 2014), a recently developed fully three dimensional radiative transfer code, which computes the dust reprocessing of the primary photons emitted by stellar populations (or other sources). GRASIL-3D, while largely based on the formalism of the widely used model GRASIL (Silva et al. 1998; Granato et al. 2000), has been specifically designed to be applied to systems with arbitrary geometry, where radiative transfer through dust plays an important role, such as galaxies or interesting regions identified in the output of hydrodynamical galaxy formation codes. With respect to the already published version, we have introduced here a few modifications, to adapt it to the output of our version of GADGET-3, in particular

¹ The virial radius and the virial mass are defined as the radius and the mass of the sphere encompassing a mean density equal to the over-density of virialization, as predicted by the spherical collapse model, and for the cosmology adopted in this paper (Bryan & Norman 1998).

for what concerns the radiative effect of AGN activity. The main features of GRASIL-3D are summarized below, while we refer the reader to Domínguez-Tenreiro et al. (2014) for all the details. A description of the modifications introduced for the purposes of this paper follows this summary.

A somewhat overlooked point is that any sensible computation of radiative transfer from the output of cosmological simulations, inevitably requires the introduction of a few more free or uncertain parameters, with respect to those already demanded by the treatment of baryon physics in the simulation itself. These are related to the sub-resolution astrophysics, in particular that concerning the molecular clouds (MCs). Since MCs are the sites of star formation, and massive stars spend part of their lives within or close to them, it is expected and well assessed that in star forming systems an important fraction of dust reprocessing occurs precisely in MCs, and this fraction is an increasing function of the specific star formation activity, and of the total reprocessing itself (e.g. Silva et al. 1998; Granato et al. 2000). Current cosmological hydro-dynamical simulations that follow galaxy formation are only beginning to resolve MCs (we remind that the typical sizes and masses of giant MCs are of the order of $\sim 10 - 20$ pc and $10^5 - 10^6 M_\odot$ respectively), for zoom-in simulations of single galaxies (e.g. Hopkins et al. 2014), but their high computational cost makes them un-doable as yet for simulations on cluster scales. Therefore in general some further sub-resolution modelling is required to cope with dust reprocessing.

In particular, in GRASIL-3D the ISM is divided into two components, the molecular clouds (MCs) and the diffuse *cirrus*. In order to calculate the mass in the form of molecular clouds, it is assumed that unresolved gas densities at any point of the simulated volume follow a log-normal probability distribution function (PDF), with mean given by the local gas density and dispersion σ (a free parameter), as suggested by small scale (~ 1 kpc) simulations. Then, the local contribution to the molecular fraction is given by the fraction of the PDF above a threshold density, $\rho_{MC,thres}$. The two parameters introduced so far, which control the molecular gas fraction are, $\rho_{MC,thres}$ and σ , may reasonably range from about 0.3 to $3 M_\odot \text{ pc}^{-3}$ and from 2 to 3 respectively.

Once calculated the molecular fraction at any location of the system, GRASIL-3D takes into account the age-dependent dust reprocessing of stellar populations, arising from the fact that younger stars are associated with denser ISM environments (note that GRASIL has been the first model to do so). This is obtained assuming that stars younger than a certain time t_0 (a further parameter) are enshrouded within molecular clouds, characterized by their mass M_{MC} and radius R_{MC} . Then, the radiative transfer is treated separately in the two components, with the required accuracy. We explicitly note that, even though we apparently introduced here two more parameters M_{MC} and R_{MC} , what actually matters for the radiative transfer computation is the ratio M_{MC}/R_{MC}^2 , which therefore should be regarded as the only new parameter. A detailed non-equilibrium calculation for dust grains smaller than a given radius (150 \AA in this work) and for polycyclic aromatic hydrocarbons molecules (PAHs) is performed. Their emission is usually very important at $\lambda \lesssim 30 \text{ \mu m}$ in the cirrus component.

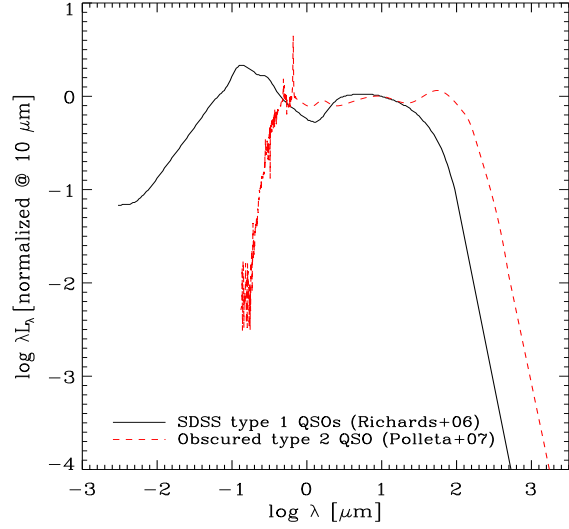


Figure 1. The SED templates adopted in this work to describe the emission of SMBH particles. In our standard computations we used the mean SED of SDSS type 1 quasars by Richards et al. 2006 (black solid line). To check the stability of our results on the IR properties of clusters, we used the very different typical SED of an obscured type 2 QSO, reported by Polletta et al. 2007 (red-dashed line).

GRASIL-3D has a general applicability to the outputs of either Lagrangian or Eulerian hydrodynamic codes. The first applications of the code have been done interfacing it with the output of the P-DEVA and GASOLINE SPH codes (Domínguez-Tenreiro et al. 2014; Obreja et al. 2014).

The main modification of GRASIL-3D introduced in this work has been to account for the radiative effect of SMBH particles present in the simulation, which provide the AGN feedback, as mentioned in Section 2. To do this, we assume that the radiation emitted by the SMBH particles is distributed according to a template SED, properly normalized by the bolometric luminosity. The latter is computed from the accretion rate and from the radiative efficiency, as $L_{bol} = \epsilon_r \dot{M} c^2$. We remind the reader that the former quantity is predicted by the simulation for each SMBH particle, while the efficiency ϵ_r is a parameter of the simulation, set to 0.2 in the runs used in this work (see Ragone-Figueroa et al. 2013, for details). As for the SED, we adopted in our standard computation the mean SED of SDSS quasars computed by Richards et al. (2006), plotted in Figure 1. It is observationally known, and theoretically expected, that AGN are characterized by a substantial anisotropy of their emission, giving rise to the broad dichotomy between type 1 and type 2 AGN. This is likely related to a preferential axis in their central engine (for a recent review see Hoenig 2013). However, we neglect this complication here. This is because of two motivations. The former is that our simulations do not give any prediction for the AGN preferential axis, which is possibly related to the SMBH spin. The second, and most reassuring one, is that we checked that different choices for the assumed template SED, even the totally opposite case of assigning to all SMBH particles the typical SED of obscured type 2 QSO, such as that reported by Polletta et al. (2007), also shown in Figure 1, yields only very small differences in

the predicted IR properties of clusters, which become usually negligible at $\lambda \gtrsim 100\mu\text{m}$ (see Section 4.2 and Figure 5).

We note that these observational templates include by construction the reprocessing by dust in the region close to the SMBH, namely that which has been since long ascribed to a torus-like structure. The latter has been invoked to explain the observational differences between type 1 (*un-obscured*) and type 2 (*obscured*) AGNs (e.g. Pier & Krolik 1993; Granato & Danese 1994; Efstathiou & Rowan-Robinson 1995). This is actually what we need. Indeed, even though little can still be safely concluded on the detailed geometrical properties of these structures (e.g. Hoenig 2013, and references therein), even the more extended models do not consider torii larger than $\sim 200 (L_{\text{AGN}}/(10^{46}\text{erg s}^{-1}))^{1/2}$ pc (Granato, Danese, & Franceschini 1997), which is far below the resolution of any cosmological simulation.

We assumed that SPH gas particles contain dust only when their temperature is lower than a certain threshold, that in the present work we set to 10^5 Kelvin. However, the results are very weakly dependent on this value. For instance, we verified that the predicted SEDs of clusters are almost indistinguishable if the threshold is increased or decreased by a factor ~ 10 . The maximum difference occurs at around the peak of dust emission $\sim 100\mu\text{m}$ and in the far UV, and is $\lesssim 10\%$. The dust to gas ratio δ of gas particles colder than the threshold temperature was assumed to be proportional to the their metallicity, with a proportionality constant calibrated to get the standard galactic value $1/110$ at solar metallicity, i.e. we set $\delta = Z/(110 Z_{\odot})$. This corresponds to assuming that about 50% of metals are locked in dust grains.

4 RESULTS

The outputs of GRASIL-3D are mock images of the portion of the simulated box in which the radiative transfer has been performed, and SEDs of the radiation coming out from the same box. We have processed boxes of physical size 2 Mpc, encompassing each of the 24 clusters, at several redshift between 0.5 and 3. Figures 2 and 3 show examples of such images, in several interesting band-passes, for one of the clusters at redshift 1 and 2 respectively. The physical size of each panel is 2000 kpc, which at these redshift is close to the Planck HFI beams ~ 5 arcmin, and is larger than the virial diameter of the clusters at both redshifts, typically by a factor ~ 2 and 5 respectively. No telescope effects (like point spread functions, pixel sizes, etc.) have been taken into account. In this Section, we will show how the predicted SEDs arising from the same region depend on GRASIL-3D parameters and other assumptions, and then we will discuss some implications for star forming cluster searches at sub-mm wavelengths.

4.1 Dependence on GRASIL-3D parameters and assumptions

To summarize, the parameters introduced by the radiative transfer calculations performed with GRASIL-3D are (i) the timescale for newly born stars to get rid of the parent MC,

t_0 ; (ii) the ratio between the mass of MCs and the square of their radius $M_{\text{MC}}/R_{\text{MC}}^2$, which in conjunction with the dust to gas ratio δ determines the optical depth of the MC, $\tau \propto \delta M_{\text{MC}}/R_{\text{MC}}^2$; we remind that δ is set by the local gas metallicity, see end of Section 3; (iii) the threshold density for gas to be in the MC dense phase $\rho_{\text{mc},\text{thres}}$ and (iv) the dispersion σ of the sub-resolution PDF of gas densities. The latter two determines the fraction of gas in molecular form. Our adopted standard values for these quantities are reported in Table 1, together with their reasonable ranges (see Domínguez-Tenreiro et al. 2014, and references therein). Fig. 4 shows the SED of the same region of Fig. 2, computed under large variations of these parameters, with respect to our adopted standard values. These variations are thought to exacerbate the effects, but despite this, in the spectral region above $\sim 100\mu\text{m}$ rest frame, which is that required to compare with the observations discussed in this paper, the effects are small, and becomes negligible above $\sim 200\mu\text{m}$, while at shorter IR wavelengths, where the contribution of MC becomes important, the consequences of these different choices of parameters may be significative, and would ask for careful evaluation. In particular, for $10 \lesssim \lambda \lesssim 40\mu\text{m}$ they may amount to a factor ~ 2 .

Besides the uncertainties in GRASIL-3D outputs arising from the choice of its explicit parameters, there are also those related to the adopted optical properties of dust grains, which are by far less understood and predictable than commonly assumed (for a recent review see Jones 2014). In this work we retain the same dust mixtures for the MCs and for the cirrus as in Domínguez-Tenreiro et al. (2014), which have been calibrated to reproduce the average properties of local galaxies. As for computing dust emission, the most delicate region is that below $\sim 30\mu\text{m}$, where the contribution from small thermally fluctuating grains and PAHs becomes important, and relatively minor variations just in the adopted size distribution of grains may produce large variations. This kind of uncertainty is expected to increase with redshift, and considering environments very different from those in which our knowledge of dust optical properties has been derived. At longer wavelengths, where the bulk of IR power is normally emitted, and is dominated by grains big enough to be in thermal equilibrium with the radiation field, the predictions are much more robust. Here, the largest source of uncertainty is possibly the wavelength decline of the grain absorption coefficient. The *canonical* computations by Draine & Lee (1984), used in this work, yields a power-law decline $\propto \lambda^{-\beta}$ with $\beta = 2$ for $\lambda \gtrsim 40\mu\text{m}$, however several laboratory measurements suggest a temperature dependence of β , with $1.5 < \beta < 2.5$ (see discussion and references in Jones 2014). Specifically, the possibility $\beta < 2$ has been sometimes welcomed, in order to help in the well known difficulty of galaxy formation models in reproducing the high levels of bright sub-mm number counts (e.g. Baugh et al. 2005).

A detailed study of the dependence of IR properties of simulated clusters on dust properties is beyond the scope of this exploratory study. However, in view of the discussion of Section 4.3, which exploit the expected luminosity in the spectral range $\sim 100 - 400\mu\text{m}$ rest frame, we checked that adopting the extreme value $\beta = 1.5$ the SED is essentially unaffected below $100\mu\text{m}$, and above this wavelength the

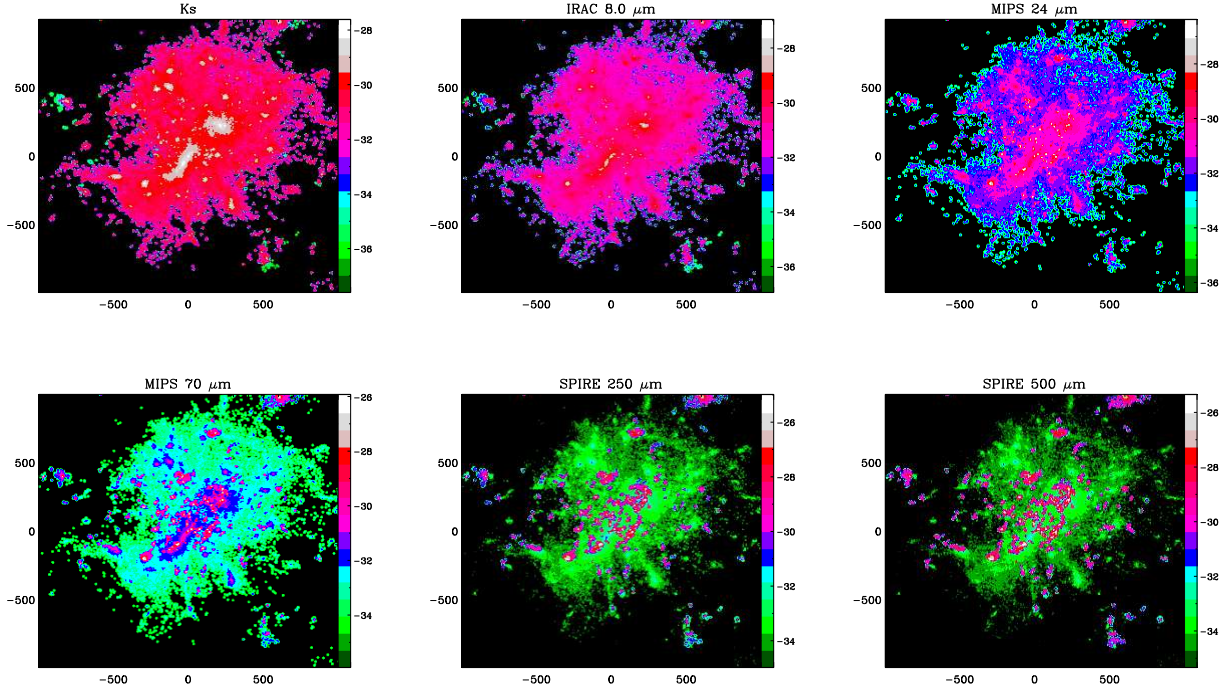


Figure 2. Examples of images of a cluster region at $z=1$ produced by GRASIL-3D in various NIR to sub-mm bands. The flux units are logarithm of $\text{erg s}^{-1} \text{cm}^{-2} \text{Hz}^{-1} \text{arcsec}^{-2}$. The physical size of each panel is 2000 kpc, close to the Planck HFI beam at that redshift. No telescope effects (like point spread functions, pixel sizes, etc.) have been taken into account.

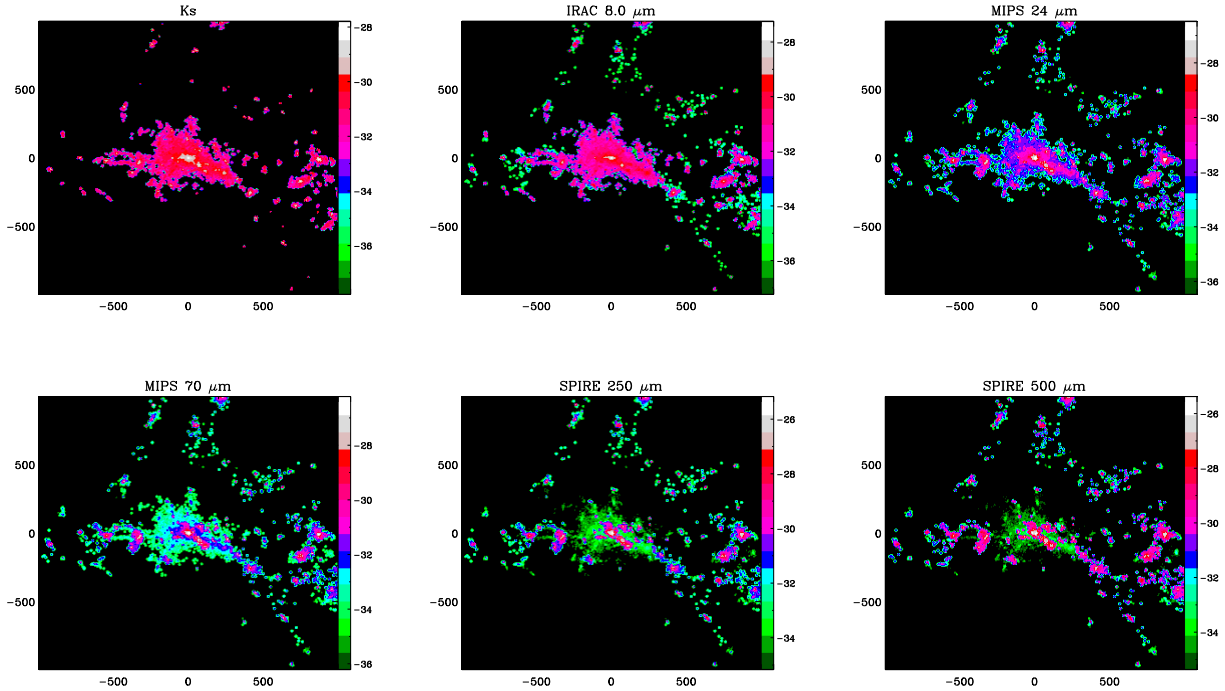


Figure 3. Same as Fig. 2 but at $z=2$

expected luminosity is progressively enhanced, typically by about 30-40% at $400 \mu\text{m}$. This moderate increase would not affect any of our conclusion.

4.2 The radiative effect of SMBHs

Fig. 5 and Fig. 6 highlight the radiative contribution of the SMBHs particles to the SEDs. The former one shows a comparison of the SEDs obtained including or not their effect, for a couple of clusters seen at $z=1$ and 2. Also, the SEDs are computed for two very different AGN templates (shown

| Parameter | Adopted value | Reasonable range | Short description |
|-------------------|---|---|--|
| t_0 | 6 Myr | 1 to 30 Myr | Escape timescale of stars from parent MCs |
| M_{MC}/R_{MC}^2 | $5 \times 10^5 \text{ M}_\odot / (10 \text{ pc})^2$ | $10^5 \text{ to } 10^6 \text{ M}_\odot / (10 \text{ pc})^2$ | Determines MCs optical depth |
| $\rho_{MC,thres}$ | $1 \text{ M}_\odot / \text{pc}^3$ | $0.3 \text{ to } 3 \text{ M}_\odot / \text{pc}^3$ | Threshold density for gas to be considered in MC phase |
| σ | 2.5 | 2 to 3 | Dispersion of the sub-resolution PDF of gas densities |

Table 1. Parameters introduced by GRASIL-3D computation.

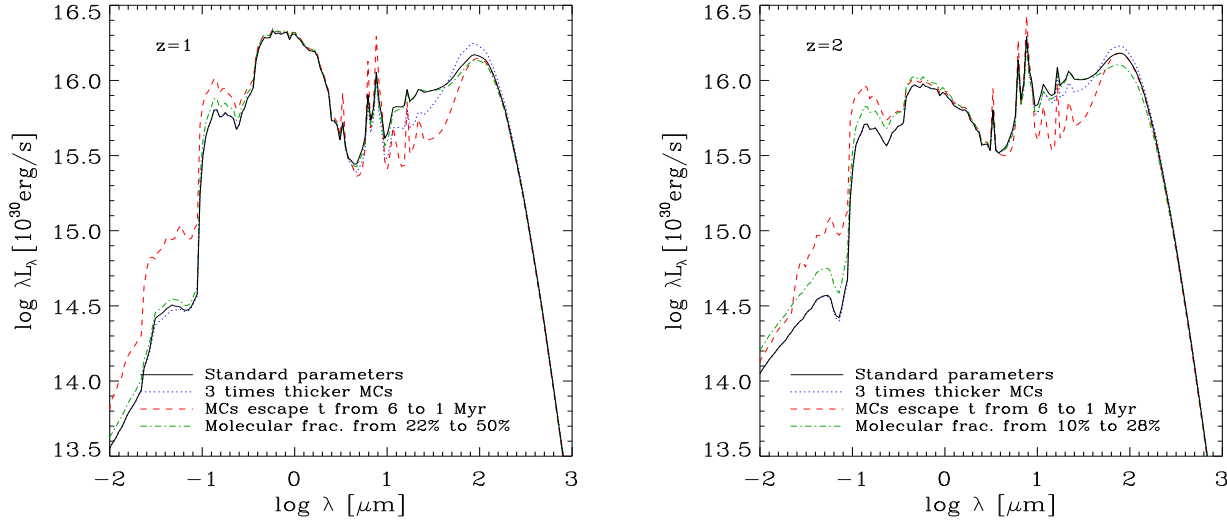


Figure 4. Comparison of the rest frame SED obtained for one cluster at $z=1$ and 2 , with different choices of GRASIL-3D parameters. Solid-black: standard values; blue-dotted: increasing the mass of individual MCs (and thus their optical depth) by a factor 2; red-dashed: decreasing the escape timescale of stars from MC by a factor 6 (from 6 to 1 Myr); green-dot-dashed: decreasing the threshold for gas to be in the dense MC phase by a factor 10, so that the molecular gas fraction increases from about 22% to about 50% at $z=1$ and from about 10% to 28% at $z=2$. In any case, the SEDs are very little affected above $\lambda \gtrsim 100 \mu\text{m}$, which is the spectral region on which we compare with observations in this paper. Note also that the parameter variations have been adopted to exacerbate the effects, but often leads to somewhat unrealistic values.

in Figure 1; see Section 3). The latter figure displays the median ratio, the 25% and the 75% percentiles of the predicted fluxes including or excluding the radiative effect of AGNs, for all the sample. We note explicitly that in both cases we are considering the same simulations in which the AGN feedback is included. Usually, in the spectral ranges between 0.1 to $1 \mu\text{m}$ and 15 to $100 \mu\text{m}$, we found that the AGN activity boost the integrated flux by a fraction ranging from $\sim 10\%$ to 50% at $z=2$. Moreover, the effect tends to decrease with decreasing redshift, being often negligible at $z=1$. However, in the far UV at $\lambda \lesssim 0.1 \mu\text{m}$ and in the near IR at $2 \mu\text{m} \lesssim \lambda \lesssim 15 \mu\text{m}$ its contribution becomes more significant. In the former regime, this is due to the fact that QSOs are believed to emit a significantly harder spectrum than the stars below the Lyman limit, but the detailed result is strongly dependent on the adopted AGN template (this is the main reason why this range is not shown in Fig. 6). In the latter spectral regime, the reason is that only very concentrated and extremely luminous sources may produce an interstellar radiation field so intense to heat dust grains at $T \sim 1000 \text{ K}$, which is required to get a thermal emission peaking at λ a few μm . As a result, at $\lambda \sim 3 \mu\text{m}$, the AGNs often boost the predicted flux by a factor of a few. On the

other hand, at $\lambda \gtrsim 100 \mu\text{m}$, the radiative effect of SMBH particles amounts to less than 25%, with our chosen (as well as any reasonable) AGN SED template.

4.3 Sub-mm properties of the clusters

In the previous sections we have seen that in the far-IR $\lambda \gtrsim 100 \mu\text{m}$, the uncertainties introduced by the sub-resolution modelling of the radiative transfer in the MCs are negligible, and the dust emission is mostly powered by star formation, with a tiny contribution from AGN activity. These are interesting points in view of efficiency of far-IR/sub-mm surveys in detecting high- z objects in a violent, dust obscured, star forming phase (e.g. Coppin et al. 2006, and references therein). Indeed, it has been proposed to take advantage of large area surveys performed in this spectral region to uncover pristine evolutionary phases of cluster regions, undergoing simultaneous star-bursts (e.g. Negrello et al. 2005).

In this vein, Clements et al. (2014) have recently reported the potential detection of four clusters of dusty, star forming galaxies at photometric redshift 0.76, 1.04, 2.05 and 2.26, by examining the Herschel-SPIRE images of Planck

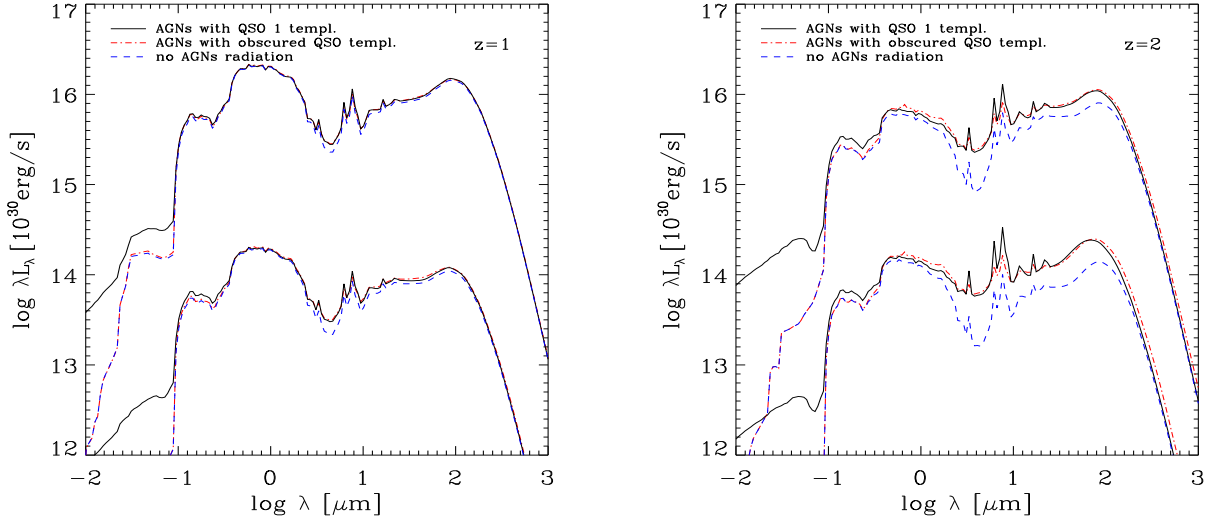


Figure 5. Comparison of the rest frame SED obtained for two clusters at $z=1$ and 2 , by including or neglecting the radiative effect of AGNs, or by adopting different templates for it. The three lower lines have been artificially displaced by a factor ten, and refer to a rare case ($\sim 10\%$ at $z=2$, but never at $z=1$) in which the differences are most prominent (at $z=2$), while the three upper lines refer to the same cluster considered in Fig.4, which is more typical. Solid-black: including the radiative effect of AGNs with our standard template, namely the mean SED of SDSS quasars by Richards et al. (2006); blue-dashed: neglecting the radiation emitted by AGNs; red-dot-dashed: including the radiative effect of AGNs, but using the template by Polletta et al. (2007) for heavily obscured type 2 QSOs.

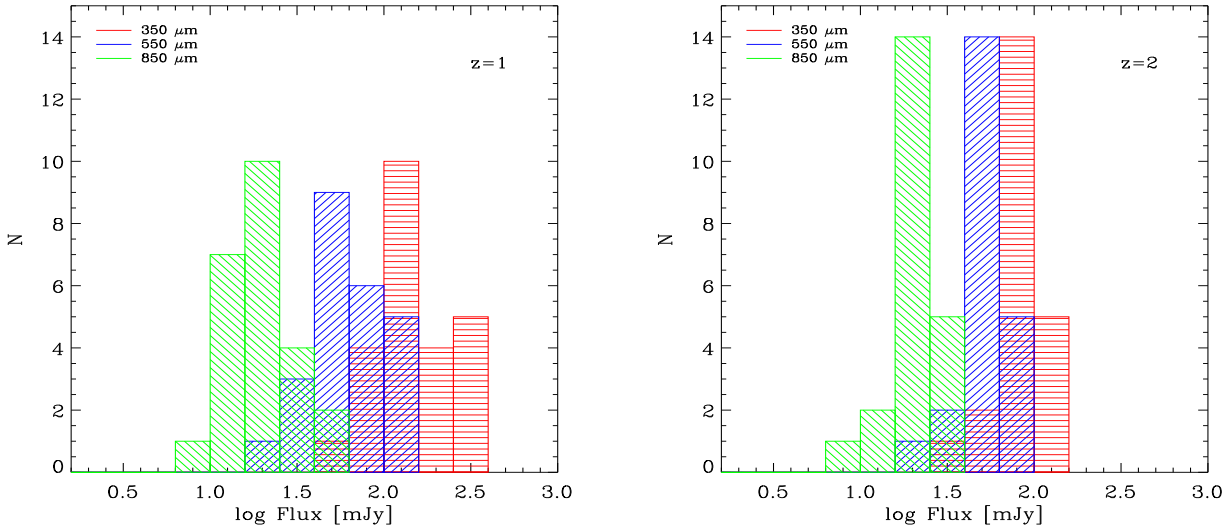


Figure 7. Distributions of the predicted fluxes from our sample of simulated clusters, within the Planck beam (~ 5 arcmin FWHM) in the 350 , 550 and $850 \mu\text{m}$ HFI bands (857 , 545 and 353 GHz respectively). The four candidate proto-clusters selected by Clements et al. 2014 have photometric redshift of 0.76 , 1.04 , 2.05 , and 2.26 and $350 \mu\text{m}$ HFI fluxes of 1100 , 810 , 1250 and 1240 mJy, i.e. close to the right bound of these plots. However, these fluxes are believed to be overestimated by a factor 2 to 3 due to selection bias. See text for details and discussion.

Early Release Compact Source Catalog sources covering an area of about 90 sq. degrees. With our panchromatic computation of the expected SED of the most massive cluster regions simulated in a large cosmological box, it is interesting to check to what extent these detections fit in our simulations. In this respect, it is worth pointing out that the comoving volume encompassed by the 90 sq. deg. area over

the $z = 0.76 - 2.3$ redshift range, is of about $0.6 h^{-1} \text{ Gpc}^3$ for the adopted cosmology, thus smaller than the comoving volume of the parent simulation.

The measured Planck fluxes of the four cluster are all of the order of $\sim 10^3$ mJy at $350 \mu\text{m}$ (857 GHz). However, as mentioned by the authors themselves, it must be taken into account that Planck fluxes fainter than 1.3 Jy are flux-

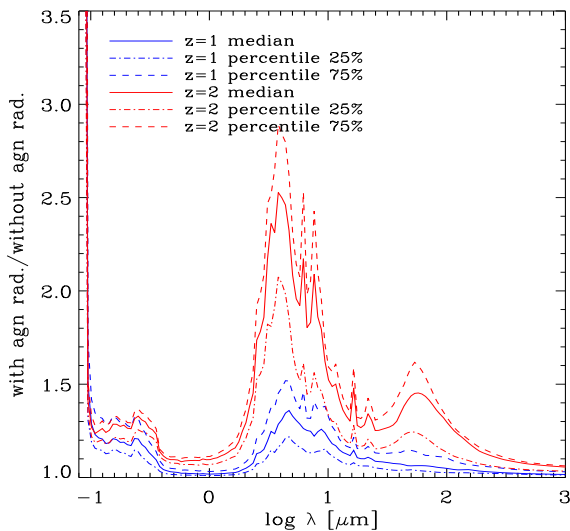


Figure 6. Ratio of the predicted fluxes including or excluding the radiative effect of AGNs, as a function of wavelength λ (rest frame), for our standard choice of GRASIL-3D parameters. Above $\sim 100 \mu\text{m}$ the difference is in most cases $\lesssim 25\%$, decreasing with increasing λ .

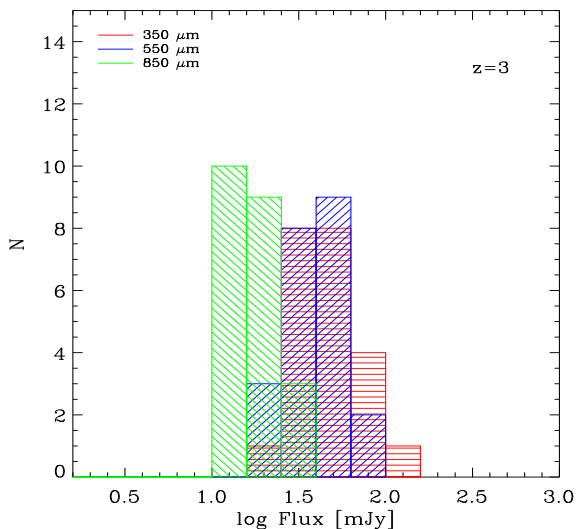


Figure 8. Same as Figure 7, but at $z=3$

boosted, due to the well known selection bias of faint sources sitting on top of positive noise (Herranz et al. 2013), and indeed they found that the sum of the fluxes of the Herschel sources in the Planck beam are typically lower by a factor 2-3. Histograms of the predicted fluxes in the Planck bands for our sample of mock clusters are shown in Figs. 7 and 8. The median expected flux is of about 131 and 85 mJy at $z=1$ and 2 respectively, but there are cases reaching ~ 300 and 100 mJy respectively. Thus we can conclude that the expected fluxes could marginally explain those reported by Clements et al. for the two sources $z \sim 1$, taking into account somewhat generously of flux boosting, while they fail to do so by a

significant factor $\gtrsim 3-4$ for the other two sources at $z \sim 2$. Indeed, while Clements et al. (2014), by considering the sum of the fluxes of Herschel sources within the Planck beam, estimate for their two $z \simeq 2$ clumps SFRs of $\sim 4.9 \times 10^3$ and $1.2 \times 10^4 \text{ M}_\odot \text{ yr}^{-1}$, none of our simulated cluster has a SFR exceeding $1700 \text{ M}_\odot \text{ yr}^{-1}$ ($1300 \text{ M}_\odot \text{ yr}^{-1}$ within the virial radius) within the same beam, with median value of $1000 \text{ M}_\odot \text{ yr}^{-1}$ ($800 \text{ M}_\odot \text{ yr}^{-1}$ within the virial radius), as measured directly on the simulations output. It is also interesting to point out that very recently Dannerbauer et al. (2014), using APEX-LABOCA observations at $870 \mu\text{m}$, determined a SFR of $\gtrsim 6300 \text{ M}_\odot \text{ yr}^{-1}$ within a region of the same size $\sim 2 \text{ Mpc}$, around the protocluster region traced by the *spiderweb* radiogalaxy at $z = 2.16$, similar to that estimated by Clements et al., for their clumps at $z \sim 2$. We recall that, as discussed in Section 4.2, the contribution from AGN power to the flux in the spectral region covered by Planck is minimal for our simulated clusters. On the other hand, for the other two observed clumps, whose photometric redshifts are 0.76 and 1.04, the SFR estimates are ~ 600 and $1600 \text{ M}_\odot \text{ yr}^{-1}$ respectively. These figures can marginally fit with the SFRs in our sample at $z=1$, whose median is 570 and maximum $1600 \text{ M}_\odot \text{ yr}^{-1}$.

Fig. 9 shows the contribution expected from our simulated clusters to the cumulative number counts, as unresolved sources, in the Planck HFI bands. They have been computed properly integrating in redshift the luminosity functions evaluated at several redshift between 0.5 and 3. As expected from the previous discussion, they do not show up at all at flux levels of the order of 1 Jy, and in order to find a few clusters over an area of ~ 90 square degrees, as reported by Clements et al. (2014), it would be necessary, according to our computations, to reach much lower sensitivities, $\sim 100 \text{ mJy}$ at $350 \mu\text{m}$. This is far too low even for the typical sensitivity $\sim 0.7 \text{ Jy}$ of the last Planck catalogues of compact sources (Planck Collaboration et al. 2013).

In Figure 10 we show the predicted $z=2$ images in the Herschel-SPIRE $350 \mu\text{m}$ band for two cluster regions. These are the two regions characterized by the highest SFR in our sample at that redshift, $\sim 1600 \text{ M}_\odot \text{ yr}^{-1}$ within the box, and have been convolved with a gaussian PSF of 25 arcsec FWHM, corresponding to the telescope diffraction limit. As can be judged by these maps, the brightest simulated clusters are expected to produce just a few almost unresolved sources, whose total flux in the beam is close to the Herschel confusion limit at this wavelength $\sim 6 \text{ mJy}$ (Nguyen et al. 2010).

In conclusion, it would be very difficult, if not impossible, to uncover and study structures similar to those predicted by our simulations with present day FIR and sub-mm space facilities.

As we mentioned before, we have also simulation runs with AGN feedback switched off. In this case the predicted SFRs, and correspondingly the expected fluxes in the Herschel bands, are typically higher by a factor ~ 2 and 1.5 at redshift 1 and 2 respectively. These numbers would be in better agreement with the figures quoted by Clements et al. (2014), albeit still too low at $z \sim 2$. Moreover, it is well known that without some treatment of this astrophysical process, cosmological simulations over-predict the amount of baryons converted into stars, particularly in massive sys-

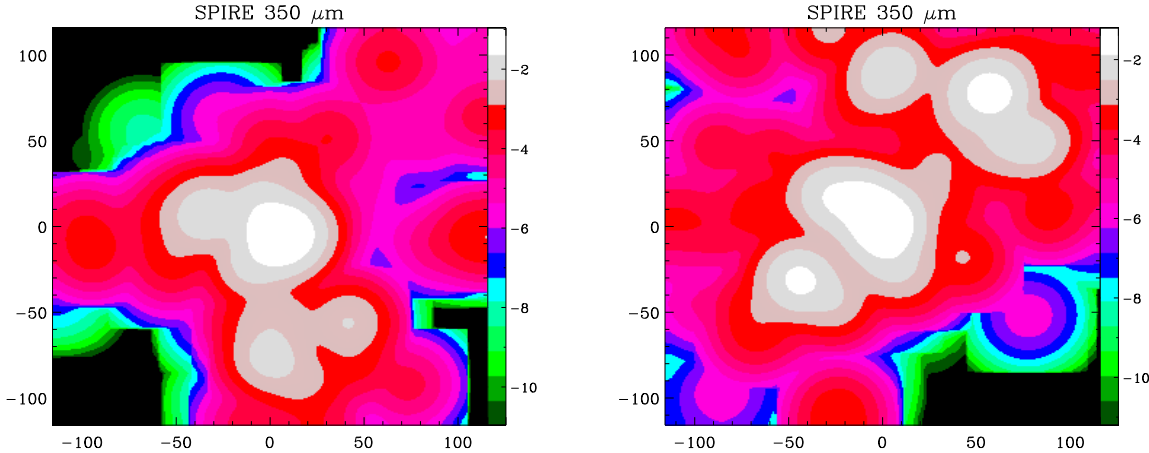


Figure 10. Images of the two cluster regions having the highest SFR at $z=2$ (at that redshift) of our sample, namely $\sim 1600 \text{ M}_{\odot} \text{ yr}^{-1}$ within the box, produced by GRASIL-3D in the Herschel-SPIRE $350 \mu\text{m}$ band, and convolved with a gaussian PSF having of 25 arcsec FWHM, corresponding to the telescope diffraction limit. The color coded flux units are logarithm of mJy arcsec^{-2} , and the numbers on the horizontal and vertical left axes marks arcsec. The physical size of each panel is 2000 kpc, close to the Planck HFI beam at that redshift.

tems, by about one order of magnitude (see for instance Ragone-Figueroa et al. 2013, and references therein).

5 SUMMARY AND CONCLUSIONS

In this work, we have post-processed a sample of cosmological zoom-in simulations following the formation of the 24 most massive galaxy clusters selected from a parent simulation of box size of $1h^{-1} \text{ Gpc}$. The final virial mass of the clusters ranges from $\simeq 1$ to $3 \times 10^{15} h^{-1} \text{ M}_{\odot}$. The post processing consists in performing radiative transfer computations with the GRASIL-3D code (Domínguez-Tenreiro et al. 2014) including dust reprocessing, in order to predict the IR properties of the forming clusters during the most active star forming phases. We have implemented in GRASIL-3D a treatment of the radiative contribution due to AGN activity, consistent with the prescriptions adopted in the simulation for the AGN feedback. The latter is widely recognized as a key ingredient to limit the overproduction of stars in massive halos. The expected contribution to the IR emission from accretion power could be significant at $\lambda \lesssim 100 \mu\text{m}$, but minor or negligible at $\lambda \gtrsim 100 \mu\text{m}$. However, going to shorter and shorter wavelengths, the exact budget becomes progressively dependent on the adopted GRASIL-3D assumptions.

We have demonstrated that during the early phases of assembly of massive galaxy clusters, our simulations do not reach far IR luminosities high enough, by a factor at least of a few, to explain the reported discovery of four high z , massively star forming clusters by Clements et al. (2014), over an area of about 90 sq. degrees in the Planck satellite survey. Since we have shown that this conclusion is very robust with respect to any reasonable variation of the assumptions required to perform the dust emission computations, and that the possible contribution to the overall emission from AGN is small in this spectral regime, the problem directly translates to *insufficient peaks* of star formation activity in the simulations at early epochs. This problem becomes more puzzling taking into account that the same simulations overpredict the final stellar mass in BCGs hosted by massive

clusters at $z=0$, by a factor of a few (Ragone-Figueroa et al. 2013).

High-redshift star formation rate can be increased in numerical simulations. Improving the resolution would already boost the SFR to some extent (e.g. Borgani et al. 2006), but still not enough to eliminate the tension between observations and the models. Besides, it would be possible to recalibrate the sub-grid prescriptions for the baryon physics. However, it appears very difficult to enhance the SFR at high redshifts without also increasing the final mass of simulated BCGs, thus worsening the above mentioned disagreement.

Moreover, recent observations suggest a picture according to which the $z \gtrsim 1.5$ population of galaxy (proto)clusters contains examples with both extreme (e.g. Tran et al. 2010; Clements et al. 2014; Dannerbauer et al. 2014; Santos et al. 2014a,b) as well as very low star formation activity (e.g. Tanaka et al. 2013; Kubo et al. 2014), while in our simulated clusters these two opposite situations are clearly under-represented. It seems that the bulk of star formation in the progenitors of real massive galaxy clusters occurred at higher rates, but lasted less than in our simulations.

These opposite tensions may indicate that the prescriptions adopted to describe the sub-resolution processes should be improved to better capture the relevant physics. Possibly, if the situation hinted by the growing data set on (proto)clusters at $z \gtrsim 1$ is confirmed, the interplay between the feedback schemes and the star formation model should yield overdense regions characterized by both higher and lower star formation levels than attained in current simulations, while avoiding an overproduction of stars over the assembly history of the most massive cluster galaxies. It is conceivable that an early phase of positive feedback during the development of AGN activity (e.g. Silk 2013), and/or a longer delay between the most violent episodes of star formation and the onset of efficient AGN quenching (e.g. Granato et al. 2004), could be part of a more realistic modeling.

Finally, we notice that since our prescriptions for the baryonic sub-grid physics, apart minor variations, are quite

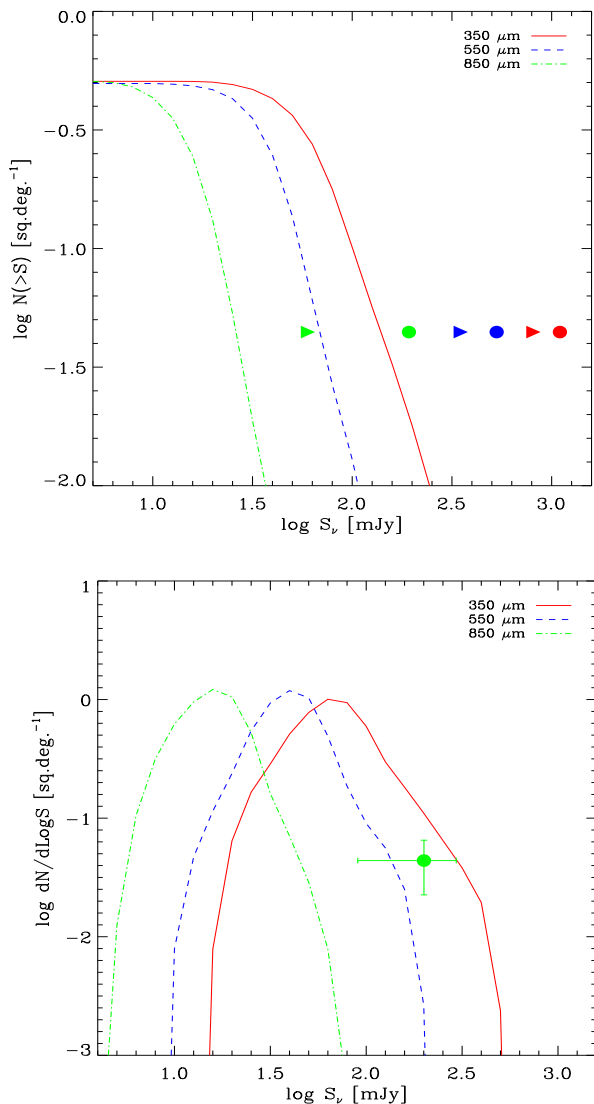


Figure 9. Expected contribution to the cumulative and differential number counts in the Planck HFI bands from the simulated clusters considered in this work, namely all clusters whose final virial mass $\gtrsim 1 \times 10^{15} h^{-1} M_{\odot}$, treated as unresolved sources.

In the upper panel, the colored circles (triangles) mark the position corresponding to the average (minimum) fluxes and the number density suggested by the four Planck clumps detected by Clements et al. 2014, over an area of 90 square degrees. In the lower panel, the circle with error bars is the estimate given by these authors at $850 \mu\text{m}$.

standard in present day cosmological simulations, we expect that our findings would apply to most of them in the same halo mass regime.

ACKNOWLEDGEMENTS

G.L.G. acknowledges warm hospitality by IATE-Córdoba during the development of the present work. The authors thank Volker Springel for making available to us the non-public version of the GADGET3 code. Simulations have

been carried out at the CINECA supercomputing Centre in Bologna, with CPU time assigned through ISCRA proposals and through an agreement with University of Trieste. C.R.F. acknowledges founding from the Consejo Nacional de Investigaciones Científicas y Técnicas de la República Argentina (CONICET), by the Secretaría de Ciencia y Técnica de la Universidad Nacional de Córdoba (SeCyT) and by the Fondo para la Investigación Científica y Tecnológica (FonCyT). This work has been supported by the PRIN-MIUR 201278X4FL Evolution of cosmic baryons funded by the Italian Ministry of Research, by the PRIN-INAF09 project Towards an Italian Network for Computational Cosmology, and by the INDARK INFN grant, by the MICINN and MINECO (Spain) through the grants AYA2009-12792-C03-03 and AYA2012-31101 from the PNAyA and by the European Commission's Framework Programme 7, through the International Research Staff Exchange Program LACEGAL. A.O. was financially supported through a FPI contract from AYA2009-12792-C03-03.

REFERENCES

- Baugh C. M., Lacey C. G., Frenk C. S., Granato G. L., Silva L., Bressan A., Benson A. J., Cole S., 2005, *MNRAS*, 356, 1191
- Bonafede A., Dolag K., Stasyszyn F., Murante G., Borgani S., 2011, *MNRAS*, 418, 2234
- Borgani S., et al., 2006, *MNRAS*, 367, 1641
- Bryan G. L., Norman M. L., 1998, *ApJ*, 495, 80
- Camps P., Baes M., 2014, *arXiv*, arXiv:1410.1629
- Chakrabarti S., Whitney B. A., 2009, *ApJ*, 690, 1432
- Clements D. L., et al., 2014, *MNRAS*, 439, 1193
- Cooper M. C., et al., 2008, *MNRAS*, 383, 1058
- Coppin K., et al., 2006, *MNRAS*, 372, 1621
- Dannerbauer H., et al., 2014, *A&A*, 570, A55
- Domínguez-Tenreiro R., Obreja A., Granato G. L., Schurer A., Alpresa P., Silva L., Brook C. B., Serna A., 2014, *MNRAS*, 439, 3868
- Draine B. T., Lee H. M., 1984, *ApJ*, 285, 89
- Efstathiou A., Rowan-Robinson M., 1995, *MNRAS*, 273, 649
- Elbaz D., et al., 2007, *A&A*, 468, 33
- Fassbender R., et al., 2014, *A&A*, 568, A5
- Gobat R., et al., 2013, *ApJ*, 776, 9
- Granato G. L., Danese L., 1994, *MNRAS*, 268, 235
- Granato G. L., Danese L., Franceschini A., 1997, *ApJ*, 486, 147
- Granato G. L., Lacey C. G., Silva L., Bressan A., Baugh C. M., Cole S., Frenk C. S., 2000, *ApJ*, 542, 710
- Granato G. L., De Zotti G., Silva L., Bressan A., Danese L., 2004, *ApJ*, 600, 580
- Guo Q., et al., 2011, *MNRAS*, 413, 101
- Hatch N. A., Kurk J. D., Pentericci L., Venemans B. P., Kuiper E., Miley G. K., Röttgering H. J. A., 2011, *MNRAS*, 415, 2993
- Hayashi M., Kodama T., Koyama Y., Tadaki K.-I., Tanaka I., 2011, *MNRAS*, 415, 2670
- Herranz D., et al., 2013, *A&A*, 549, A31
- Hilton M., et al., 2010, *ApJ*, 718, 133
- Hoenig S. F., 2013, *arXiv*, arXiv:1301.1349

- Hopkins P. F., Kereš D., Oñorbe J., Faucher-Giguère C.-A., Quataert E., Murray N., Bullock J. S., 2014, *MNRAS*, 445, 581
- Inagaki T., Lin Y.-T., Huang H.-J., Hsieh B.-C., Sugiyama N., 2014, *arXiv*, arXiv:1409.4820
- Jones A., 2014, *arXiv*, arXiv:1411.6666
- Jonsson P., Groves B. A., Cox T. J., 2010, *MNRAS*, 403, 17
- Johansson P. H., Naab T., Ostriker J. P., 2012, *ApJ*, 754, 115
- Kravtsov, Andrey V., Borgani, Stefano, 2012, *ARA&A*, 50, 353
- Kubo M., Yamada T., Ichikawa T., Kajisawa M., Matsuda Y., Tanaka I., 2014, *arXiv*, arXiv:1411.2663
- Li Y., et al., 2008, *ApJ*, 678, 41
- Lidman C., et al., 2012, *MNRAS*, 427, 550
- Lin Y.-T., Brodwin M., Gonzalez A. H., Bode P., Eisenhardt P. R. M., Stanford S. A., Vikhlinin A., 2013, *ApJ*, 771, 61
- Mei S., et al., 2009, *ApJ*, 690, 42
- Negrello M., González-Nuevo J., Magliocchetti M., Moscardini L., De Zotti G., Toffolatti L., Danese L., 2005, *MNRAS*, 358, 869
- Nguyen H. T., et al., 2010, *A&A*, 518, L15
- Obreja A., Brook C. B., Stinson G., Domínguez-Tenreiro R., Gibson B. K., Silva L., Granato G. L., 2014, *MNRAS*, 442, 1794
- Pier E. A., Krolik J. H., 1993, *ApJ*, 418, 673
- Planelles S., Borgani S., Fabjan D., Killedar M., Murante G., Granato G. L., Ragone-Figueroa C., Dolag K., 2014, *MNRAS*, 438, 195
- Planck Collaboration, et al., 2013, *arXiv*, arXiv:1303.5088
- Polletta M., et al., 2007, *ApJ*, 663, 81
- Ragone-Figueroa C., Granato G. L., 2011, *MNRAS*, 414, 3690
- Ragone-Figueroa C., Granato G. L., Abadi M. G., 2012, *MNRAS*, 423, 3243
- Ragone-Figueroa C., Granato G. L., Murante G., Borgani S., Cui W., 2013, *MNRAS*, 436, 1750
- Richards G. T., et al., 2006, *ApJS*, 166, 470
- Rigby E. E., et al., 2014, *MNRAS*, 437, 1882
- Silk J., 2013, *ApJ*, 772, 112
- Silva L., Granato G. L., Bressan A., Danese L., 1998, *ApJ*, 509, 103
- Santos J. S., et al., 2011, *A&A*, 531, L15
- Santos J. S., et al., 2014, *MNRAS*, 438, 2565
- Santos J. S., et al., 2014, *arXiv*, arXiv:1412.5188
- Springel V., 2005, *MNRAS*, 364, 1105
- Springel V., Di Matteo T., Hernquist L., 2005, *MNRAS*, 361, 776
- Stott J. P., Collins C. A., Burke C., Hamilton-Morris V., Smith G. P., 2011, *MNRAS*, 414, 445
- Strazzullo V., Pannella M., Owen F. N., Bender R., Morrison G. E., Wang W.-H., Shupe D. L., 2010, *ApJ*, 714, 1305
- Strazzullo V., et al., 2013, *ApJ*, 772, 118
- Tanaka M., et al., 2013, *ApJ*, 772, 113
- Tormen G., Bouchet F. R., White S. D. M., 1997, *MNRAS*, 286, 865
- Tran K.-V. H., et al., 2010, *ApJ*, 719, L126